Generation mechanisms of active free radicals during ciprofloxacin degradation in the ultrasonic/$K_2S_2O_8$ system

Yanrui Cui, Xiaopeng Yan, GuangZhe Han, Bin Lin, Qing Wu, Wei Kang and Kaili Ma

ABSTRACT

Ciprofloxacin (CIP) removal efficiency in aqueous solutions in the ultrasonic (US), $K_2S_2O_8$, and US/$K_2S_2O_8$ systems was investigated. The free radical generation and action ratio were studied based on variations of $K_2S_2O_8$ concentration, ultrasonic power, pH, and the addition of isopropanol (ISP) or tert-butyl alcohol (TBA) in the US/$K_2S_2O_8$ system. The results showed that under conditions of 20 mg·L^{-1} CIP concentration, 20 mmol·L^{-1} $K_2S_2O_8$ concentration, an ultrasonic power of 360 W and pH = 7, CIP removal efficiency in the US/$K_2S_2O_8$ system was 92.20% after 180 min. The reaction in the US/$K_2S_2O_8$ system was explicitly divided into two stages: free radical generation and pollutants degradation. The ultrasonic and chain reaction facilitated enhanced generation of $SO_4^{\bullet-}$ and $HO^{\bullet}$. The presence of $K_2S_2O_8$ can promote $HO^{\bullet}$ generation and $K_2S_2O_8$ concentration also exerted a significant effect on $SO_4^{\bullet-}$ generation, however, high concentrations were not beneficial to the reaction. Quenching reactions occurred under high concentrations of $HO^{\bullet}$ and $SO_4^{\bullet-}$. During the initial stage of the reaction, $HO^{\bullet}$ played a more prominent role than $SO_4^{\bullet-}$, however, the role of $SO_4^{\bullet-}$ gradually increased as the reaction proceeded and eventually surpassed $HO^{\bullet}$.

Key words | ciprofloxacin, free radical generation mechanism, $HO^{\bullet}$, $SO_4^{\bullet-}$, US/$K_2S_2O_8$ system

Yanrui Cui (corresponding author)
Xiaopeng Yan
GuangZhe Han
Bin Lin
Qing Wu
Wei Kang
Kaili Ma
School of Environment, Key Laboratory for Yellow River and Huai River Water Environment and Pollution Control, Ministry of Education, Henan Key Laboratory of Environmental Pollution Control, International Joint Laboratory on Key Techniques in Water Treatment,
Henan Normal University,
Xinxiang 453007,
China
E-mail: *yanruicui@hotmail.com*

HIGHLIGHTS

- The pollutants degradation process in the US/$K_2S_2O_8$ system was explicitly divided into free radical generation stage and degradation stage.
- The free radical generation mechanism and the interaction between $HO^{\bullet}$ and $SO_4^{\bullet-}$ were investigated in detail.
- Evading the difficulty of $HO^{\bullet}$ and $SO_4^{\bullet-}$ *in-situ* determination, the ratio of $HO^{\bullet}$, $SO_4^{\bullet-}$ and other actions were calculated, the correctness of the mechanism was proved.

ABBREVIATIONS

AOPs	Advanced oxidation processes
HPLC	High performance liquid chromatography
PS	Persulfate
TBA	Tert-butyl alcohol
US	Ultrasonic
ISP	Isopropanol
CIP	Ciprofloxacin

INTRODUCTION

In recent years, on account of its oxidation ability and good stability, advanced oxidation processes based on $SO_4^{\bullet-}$ are considered effective technologies for degrading refractory organic contaminants (Gao *et al.* 2020). $SO_4^{\bullet-}$ has a number of advantages, such as possessing a high oxidative

doi: 10.2166/wst.2021.134

potential (2.6–3.1 V), a long lifetime, and a wide operative pH range (Yen *et al.* 2011; Zhang *et al.* 2019), resulting in enhanced reaction with pollutants. As a source of $SO_4^{-\bullet}$, persulfate (PS) can be activated by heat, ultraviolet, electromagnetic, transition metal ion, and ultrasonic (US) processes in order to generate $SO_4^{-\bullet}$ (Avetta *et al.* 2015). In addition, the stability of PS makes it convenient for transportation and preservation at room temperature (Li *et al.* 2019). At present, organic pollutant treatment by US/PS systems is considered a promising avenue for reasons of high efficiency and cleanliness (Chen & Huang 2015; Gao *et al.* 2018).

Extensive research has been conducted to determine the reaction mechanisms of pollutant degradation in US/PS systems. For example, Hao *et al.* (2014) indicated that $SO_4^{-\bullet}$ oxidation was responsible for ammonium perfluorooctanoate removal in the US/PS system, Nasseri *et al.* (2017) found that $HO^{\bullet}$ played a major role in the degradation of tetracycline in this system, and Monteagudo *et al.* (2018) studied the degradation of diclofenac in the US/PS system finding that, under the action of $SO_4^{-\bullet}$ and $HO^{\bullet}$, diclofenac was oxidized. Darsinoua *et al.* (2015) reported that bisphenol A was efficiently decomposed by the combined effects of $SO_4^{-\bullet}$ and $HO^{\bullet}$ produced by ultrasound activation of PS. Chen & Huang (2019) used the US/PS system to treat dinitrotoluene, finding that $SO_4^{-\bullet}$ served as the main oxidant. The research described above has demonstrated the type and effect of free radicals and carried out specific analysis for different reactions, but the essential law of the degradation reaction of pollutants in the US/PS system could not be revealed.

According to the above analyses, in the US/PS system, the reaction follows of a series of processes including the generation of free radicals and the degradation of pollutants. Herein, this study defines these two stages as follows: (1) free radical generation: US effects in the aqueous solution can cause the rapid formation, growth, and implosive collapse of bubbles, resulting in extreme temperature and pressure rises, facilitating the formation of oxidizing species such as $SO_4^{-\bullet}$ and $HO^{\bullet}$; (2) pollutants degradation: free radicals, such as $SO_4^{-\bullet}$and $HO^{\bullet}$, react with pollutants. It has been reported that the US/PS system includes the following equation: (1)–(10) (in Equations (1) and (2),))) refers to ultrasonic waves) (House 1962; Wang *et al.* 2015; Monteagudo *et al.* 2018):

$$S_2O_8^{2-} +))) / \text{heat} \rightarrow 2SO_4^{-\bullet} \quad (1)$$

$$H_2O +))) \rightarrow HO^{\bullet} + H^{\bullet} \quad (2)$$

$$S_2O_8^{2-} + HO^{\bullet} \rightarrow SO_4^{-\bullet} + HSO_4^{-} + O_2 \quad (3)$$

$$S_2O_8^{2-} + H^{\bullet} \rightarrow SO_4^{-\bullet} + HSO_4^{-} \quad (4)$$

$$SO_4^{-\bullet} + H_2O/OH^{-} \rightarrow SO_4^{2-} + HO^{\bullet} \quad (5)$$

$$HO^{\bullet} + HO^{\bullet} \rightarrow H_2O_2 \quad (6)$$

$$HO^{\bullet} + SO_4^{-\bullet} \rightarrow HSO_5^{-} \quad (7)$$

$$HSO_5^{-} + HO^{\bullet} \rightarrow SO_5^{-\bullet} + H_2O \quad (8)$$

$$SO_4^{-\bullet} + SO_4^{-\bullet} \rightarrow S_2O_8^{2-} \quad (9)$$

$$SO_4^{-\bullet} + S_2O_8^{2-} \rightarrow SO_4^{2-} + S_2O_8^{-\bullet} \quad (10)$$

The above two-stage process is necessary for the complete degradation of pollutants in the US/PS system, since the follow-up reactions cannot occur without the generation of free radicals. The generation of free radicals in the first stage is affected by many factors; several studies have reported that the influence of parameters such as power, oxidant concentration, and pH on the degradation of pollutants mainly relies on the influence of free radicals (Darsinoua *et al.* 2015; Ferkous *et al.* 2017; Yousefi *et al.* 2019). However, the reaction rate in the second stage shows relative stability. A previous report (Ao *et al.* 2018) showed that the reaction rate constants of $HO^{\bullet}$ and $SO_4^{-\bullet}$ with CIP were $k_{HO^{\bullet}/CIP} = 4.92 \times 10^9\ M^{-1}\ s^{-1}$ and $k_{SO4-\cdot/CIP} = 1.2 \times 10^9\ M^{-1}\ s^{-1}$, respectively. Lei *et al.* (2019) also indicated that the efficiency of oxidation in the US/PS system is attributed primarily to the generation of free radicals. Additionally, multiple studies (Sharma *et al.* 2016; Wang *et al.* 2019b; Milh *et al.* 2020) have also shown that different intermediates were produced during the reaction of pollutants with $HO^{\bullet}$ and $SO_4^{-\bullet}$, respectively. Consequently, free radical generation in the first stage is the decisive step during the degradation reaction, and only by understanding the generation mechanism of free radicals can we take effective control of the reaction. At present, the above two stages have not been divided and the mechanism of free radical generation was not realized explicitly.

In-situ determination of free radical concentration in the first stage is required to be researched. However, the generation of free radicals occurred in a dynamic environment and the free radicals showed a short survival time (Tang *et al.* 2018). There are no related reports on such methods, and quantitative efforts face great difficulties. The reaction mechanism can be shown through different reaction results, focusing on the design of the experiment and in-depth analyses of experimental phenomena in order to reveal free radical generation mechanisms. This is an effective way to

overcome the difficult problem of the *in-situ* determination of free radicals.

The main objective of this work was to reveal free radical generation mechanism, in the first stage, during CIP degradation in the US/$K_2S_2O_8$. To achieve this goal, the CIP aqueous solution was degraded in the US/$K_2S_2O_8$ system and, comparative experiments to determine influencing factors such as power, $K_2S_2O_8$ concentration, pH, and the addition of tert-butanol or isopropanol quenching agent were carried out. Furthermore, an in-depth analysis based on above experiment was conducted.

EXPERIMENTAL

Chemicals and reagents

Potassium persulfate ($K_2S_2O_8$, ≥99.5%) was purchased from Tianjin Damao Chemical Reagent Factory (Tianjin, China). Hydrogen peroxide (H_2O_2), sodium hydroxide (NaOH), sulfuric acid (H_2SO_4), tert-butyl alcohol (TBA), and isopropanol (ISP) of reagent grade were obtained from Tianjin Deen Chemical Reagent Factory (Tianjin, China). Methanol, triethylamine, and phosphoric acid of high performance liquid chromatography (HPLC) grade were purchased from Tedia Reagent Company (USA). CIP was obtained from Heilongjiang Kelun Pharmaceutical Co., Ltd (Heilongjiang, China) and its physical and chemical properties are shown in Table S1 (Supplementary data). All aqueous solutions in this study were prepared using ultrapure water (resistivity 18 MΩ·cm^{-1}) obtained from a Millipore Milli-Q system.

Experimental procedure

CIP degradation experiments were conducted in a US cell disruptor (YMNL–1000Y, Yimanei, China). As shown in Figure S1 (Supplementary data), the device contains the following parts: (1) US generator, including control panel and display screen, and (2) transducer assembly, including transducer and horn, equipped with a Φ 6 mm titanium probe. The US generator and the transducer assembly were connected by cable, and the temperature probe was directly connected to the control panel.

The experimental steps were as follows. A 100 mL CIP aqueous solution with a mass concentration of 20 mg·L^{-1} was prepared and a set amount of $K_2S_2O_8$ was added. The pH value was adjusted using 0.1 mol·L^{-1} H_2SO_4 and NaOH, and determined using a pH meter (PHS-3C, Leici, China). The CIP aqueous solution was transferred to the reaction vessel and the US cell disruptor was opened at the frequency of 25 kHz. The titanium needle was inserted 1.5–2 cm beneath the solution surface, and the titanium pulse (on/off) was set at 2 s/3 s. Under conditions of normal pressure and avoiding light, the US treatment was applied, and the temperature was monitored using a temperature probe. Samples of approximately 2 mL were collected every 30 min, and analysis was carried out immediately after sampling. Each group of experiments was repeated at least three times to acquire an average. CIP removal efficiency was calculated using Equation (11):

$$r = \frac{(C_0 - C_t) \times V}{C_0 \times V} \times 100\% \quad (11)$$

where r is CIP removal efficiency (%), C_0 and C_t are CIP mass concentration (mg·L^{-1}) at time 0 and time t, respectively, and V is the volume of the CIP solution.

Analytical methods

CIP concentrations were detected using HPLC, Waters 2695, USA) equipped with a Waters-C18 column (150 mm × 4.6 mm, 5 μm); the column temperature was set at 30 °C, and the mobile phase comprised 25% methanol and 75% 0.25 mol·L^{-1} phosphoric acid aqueous solution, which was adjusted with triethylamine to pH 3.0. The mobile phase was passed through a 0.45 μm filter membrane before use, the flow rate was set to 1 ml·min^{-1}, and the injection volume was 20 μL. The peak area was quantified using the external standard method with a maximum absorption wavelength of 278 nm for CIP and a retention time of 5.92 min.

H_2O_2 concentration was determined spectrophotometrically using the $TiCl_4$ method (Laat & Gallard 1999).

RESULTS AND DISCUSSION

Determination of active free radicals for CIP removal in the US/$K_2S_2O_8$ system

In order to determine the active free radicals produced in the US/$K_2S_2O_8$ system, the removal efficiencies of CIP in US, $K_2S_2O_8$, and US/$K_2S_2O_8$ were compared, and the effects of excessive TBA and ISP on CIP removal efficiency were investigated in the US/$K_2S_2O_8$ system. The results are shown in Figure 1.

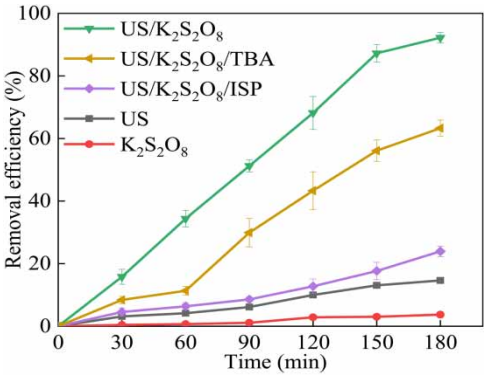

Figure 1 | Comparison of the CIP removal efficiency of different systems. Reaction conditions: CIP concentration = 20 mg·L^{-1}, frequency = 25 KHz, $K_2S_2O_8$ concentration = 20 mmol·L^{-1}, power = 360 W, pH = 7.

As shown in Figure 1, both the US and $K_2S_2O_8$ experimental groups exhibited limited ability for CIP degradation and their removal efficiencies over 180 min were only 14.63% and 3.70%, respectively. A completely different result was observed in the US/$K_2S_2O_8$ experimental group, where CIP removal efficiency was up to 92.20%. The utilization efficiency of US energy alone was very low (Song *et al.* 2006), thus a low CIP removal efficiency was observed in the US experimental group. This was also the case for the $K_2S_2O_8$ experimental group due to its stability at room temperature and slow chemical reaction rate (Matzek & Carter 2016). Thus, neither the US nor $K_2S_2O_8$ system generated a sufficient amount of active free radicals for effective participation in the reaction.

An obvious increase in removal efficiency was observed in the control group, suggesting synergism between US and $K_2S_2O_8$. It therefore became necessary to determine the nature of the active free radicals generated by this synergistic effect.

In this study, TBA and ISP were utilized as free radical quenchers to identify active free radicals in the degradation process. Previous research (House 1962; Liu *et al.* 2016; Qian *et al.* 2018) has shown that TBA, a commonly used HO$^{\bullet}$ quencher, can rapidly quench HO$^{\bullet}$, whereas ISP is able to quickly quench HO$^{\bullet}$ and $SO_4^{-\bullet}$.

It was noted that CIP removal efficiency in the TBA experimental group showed a trend of gradual acceleration with prolongation of the reaction time, reaching 63.31% in 180 min, i.e., 28.90% lower than the control group. Evidently, introducing excessive TBA as the HO$^{\bullet}$ quencher resulted in a decrease in CIP degradation efficiency, suggesting that a large amount of HO$^{\bullet}$ was produced in the US/$K_2S_2O_8$ system. Additionally, CIP degradation efficiency was higher than that of the $K_2S_2O_8$ system, indicating that free radicals other than HO$^{\bullet}$ were present.

The ISP experimental group exhibited a slow increase in CIP removal efficiency, reaching 23.94% in 180 min, i.e., 68.27% lower than that of the control group and 39.37% lower than that of the TBA experimental group; this can be explained by the elimination of both HO$^{\bullet}$ and $SO_4^{-\bullet}$, implying that a large amount of $SO_4^{-\bullet}$ was produced in addition to HO$^{\bullet}$.

The above experimental results demonstrated a synergy in the US/$K_2S_2O_8$ system, suggesting that both HO$^{\bullet}$ and $SO_4^{-\bullet}$ were generated in high quantity during the CIP degradation process. This was more than that produced by either the US or $K_2S_2O_8$ system in isolation.

HO$^{\bullet}$ generation mechanism in the US/$K_2S_2O_8$ system

Influence of ultrasound on HO$^{\bullet}$

Suslick (1990) determined that acoustic cavitation caused by US power could raise the temperature of the gas phase reaction zone to approximately 5,200 K, while the effective temperature of the liquid reaction zone reached about 1,900 K, and the partial pressure was 5.05×10^4 kPa, accompanied by a strong shock wave. The high temperatures and pressures generated during cavitation could decompose molecules, break chemical bonds, and generate free radicals. Under these conditions, H_2O molecules were decomposed into free radicals, such as HO$^{\bullet}$ and H· (Equation (2)). Therefore, in order to test the effect of ultrasonic power on HO$^{\bullet}$ generation, the effect of TBA on CIP degradation was investigated by adding TBA to the US system.

As illustrated in Figure 2, the CIP removal efficiency for HO$^{\bullet}$ in the US experimental group was 14.63%, whereas that in the TBA experimental group was only 4.78%, indicating that ultrasonic power was an important cause of HO$^{\bullet}$ generation.

Influence of chain reaction on HO$^{\bullet}$ generation

As described in the section on the influence of ultrasound on HO$^{\bullet}$, US power was an important parameter in HO$^{\bullet}$ generation. However, it was reported that only around 10% of HO$^{\bullet}$ produced by US power enters into the liquid phase to participate in the reaction. Figure 1 also shows that CIP removal efficiency in the control group was much higher than that in the US experimental group, indicating that other HO$^{\bullet}$ generation mechanisms or other free radicals

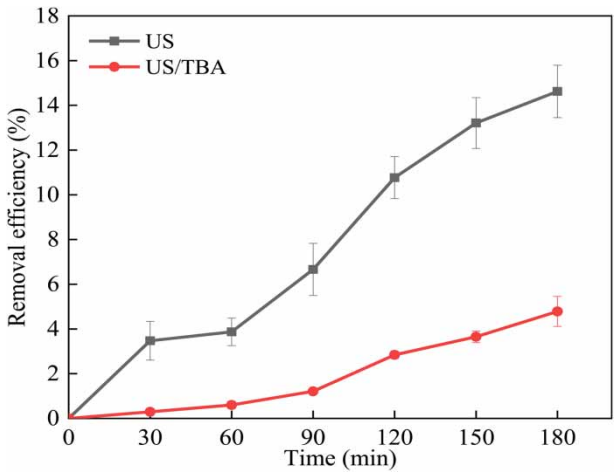

Figure 2 | The removal efficiency of CIP on the US and US/TBA systems. Reaction conditions: CIP concentration = 20 mg·L^{-1}, frequency = 25 KHz, power = 360 W, pH = 7.

were present in the US/$K_2S_2O_8$ system. Ultrasonic power between 90 W and 360 W was investigated for CIP degradation in the US/$K_2S_2O_8$ system and the HO$^{\bullet}$ generation mechanism was further analyzed. The results of this analysis are shown in Figure 3.

Figure 3(a) shows that the characteristics of CIP removal efficiency with time were significantly different under different power conditions. At powers of 90, 180, and 270 W, the rate of CIP removal efficiency increased gradually with the extension of reaction time, resulting in an upper concave curve. The higher the US power, the greater the increase in CIP removal efficiency. CIP removal efficiency in different US power experimental groups entered a plateau period after 150 min. After 180 min of reaction, CIP removal efficiency in the 90, 180, 270, and 360 W experimental groups were 86.71%, 88.46%, 90.71%, and 92.20%, respectively. Figure 3(b) shows the relationship between CIP removal efficiency and power change at different reaction times. The linear slopes at 60 and 90 min were very similar, however, this decreased after 90 min, as shown in Table S2, indicating that extended reaction times progressively reduced the effect of US power on CIP removal efficiency.

US power is thus clearly shown to promote the formation of HO$^{\bullet}$. In a certain range, higher power induces greater HO$^{\bullet}$ generation (Zhang & Zheng 2009). A similar phenomenon was observed in the US/$K_2S_2O_8$ system, such that the efficiency of CIP removal was elevated at higher power, suggesting that the presence of $K_2S_2O_8$ in the US/$K_2S_2O_8$ system had no negative impact on HO$^{\bullet}$ generation. After 150 min of reaction, no obvious differences were found between the various experimental groups: the impact of US power disappeared gradually, but a corresponding decline in removal efficiency did not occur, implying that, in addition to US power, other factors contributed to HO$^{\bullet}$ generation, or other free radicals were produced.

Free radicals produced during the activation of $K_2S_2O_8$ can initiate a series of chain reactions, such that the degradation rate of pollutants depends on the occurrence and termination of chain reactions across multiple studies (Huang *et al.* 2002; Matzek & Carter 2016). In the US/$K_2S_2O_8$ system, during the initial stages of the reaction, ultrasonic power caused hydropyrolysis, producing HO$^{\bullet}$ and H· (Equation (2)). Subsequently, HO$^{\bullet}$ and H· continued

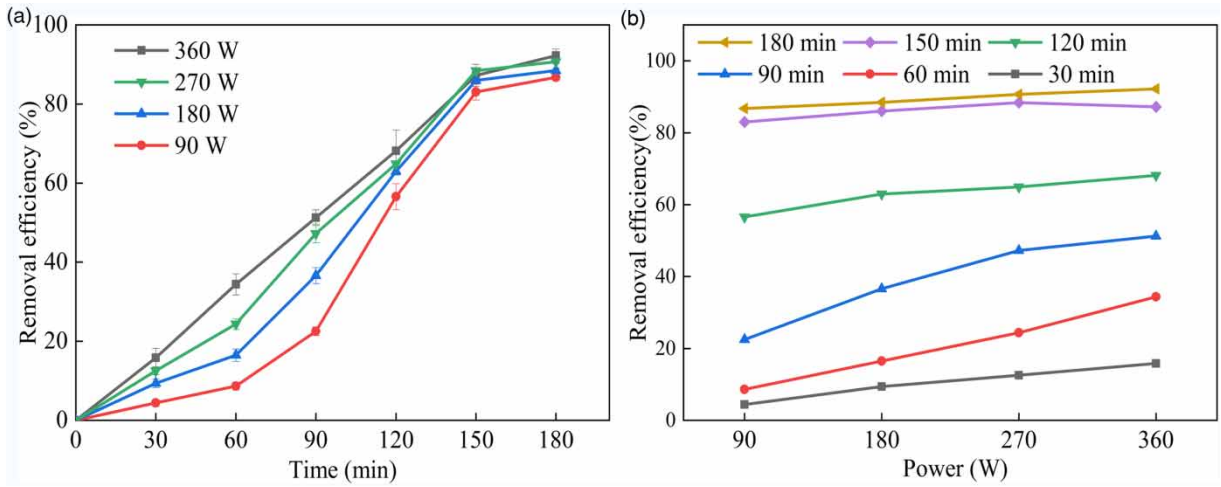

Figure 3 | (a) Relationship between the CIP removal efficiency and reaction time in the US/$K_2S_2O_8$ system with powers of 90, 180, 270, and 360 W; (b) relationship between CIP removal efficiency and power at different reaction times. Reaction conditions: CIP concentration = 20 mg·L^{-1}, frequency = 25 KHz, $K_2S_2O_8$ concentration = 20 mmol·L^{-1}, pH = 7.

to react with $K_2S_2O_8$ to form $SO_4^{\cdot-}$ (Equations (3) and (4)), which reacted with H_2O or OH^- to form $HO^{\cdot}$, as shown in Equation (5); this presented the characteristics of the chain reaction. In the above process, more $SO_4^{\cdot-}$ and $HO^{\cdot}$ would be produced in the US/$K_2S_2O_8$ system (Monteagudo *et al.* 2018).

Under conditions of 90 W, 180 W, and 270 W, during the initial stages of the reaction, removal efficiency increased slowly and the number of free radicals was low. Due to the low power used, the CIP concentration was high, leading to the consumption of free radicals such that the number of free radicals was insufficient to initiate the chain reaction. As the reaction progressed, CIP concentrations decreased gradually and free radicals gradually accumulated, eventually triggering the chain reaction, at which point the system produced more free radicals to react with CIP. Therefore, the experimental phenomenon of a concave curve appeared before 150 min. When using a power of 360 W, the generation and consumption of $HO^{\cdot}$ and $SO_4^{\cdot-}$ were close to balanced, such that the linear experimental phenomenon appeared before 150 min. Considering these analyses, it can be inferred that the chain reaction in the US/$K_2S_2O_8$ system also contributed to $HO^{\cdot}$ generation. Referring to Figure 1, after 180 min of reaction, the removal efficiency of CIP reached 92.20% in the US/$K_2S_2O_8$ experimental group and only 14.63% when only the US experimental group was considered, indicating both that the chain reaction contributed greatly to the generation of free radicals and that the existence of $K_2S_2O_8$ could promote $HO^{\cdot}$ generation.

Effect of quenching reaction on $HO^{\cdot}$

Previous literature has indicated that excessive $HO^{\cdot}$ in the system causes quenching to produce H_2O_2 (Monteagudo *et al.* 2015) following reaction (6). Changes in H_2O_2 concentration over time were measured experimentally, as shown in Figure 4. The appearance of H_2O_2 in the system indicated the presence of an $HO^{\cdot}$ quenching reaction. After 90 min, H_2O_2 concentration in the system gradually increased, suggesting that the prevalence of this quenching reaction gradually increased. The influence of power after 90 min gradually weakened with increasing reaction time as shown in Figure 3(b), consistent with the law shown in Figure 4. After 150 min, H_2O_2 concentrations decreased, suggested that the quenching reaction was inhibited; this corresponded to the time at which the removal efficiency entered the plateau phase in Figure 3(a). This decrease in $HO^{\cdot}$ concentration was the fundamental reason for the weakening of the quenching reaction and decreased CIP removal efficiency entering the plateau phase.

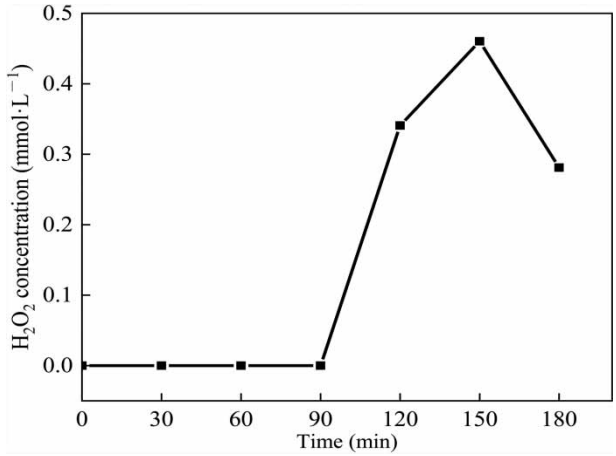

Figure 4 | Changes in H_2O_2 concentration during CIP degradation in the 360 W experimental group using the US/$K_2S_2O_8$ system.

It was demonstrated by experimental results in sections influence of ultrasound on $HO^{\cdot}$ and on the chain reaction on $HO^{\cdot}$ generation and the effect of the quenching reaction on $HO^{\cdot}$ that US power and the presence of $K_2S_2O_8$ can promote the formation of $HO^{\cdot}$, while the synergism between them produces more $HO^{\cdot}$ through the chain reaction. The quenching reaction occurs at high $HO^{\cdot}$ concentrations.

$SO_4^{\cdot-}$ generation mechanism in US/$K_2S_2O_8$

Figure 1 shows that $SO_4^{\cdot-}$ plays a greater role in the US/$K_2S_2O_8$ system than in the $K_2S_2O_8$ system. A previous study reported that US power can cause $K_2S_2O_8$ to promote $SO_4^{\cdot-}$ (Wang *et al.* 2019a). The discussion in the section on the $HO^{\cdot}$ generation mechanism in the US/$K_2S_2O_8$ system showed that both $HO^{\cdot}$ and $SO_4^{\cdot-}$ can be produced through the chain reaction. This raises the question of whether other factors also affect the generation of $SO_4^{\cdot-}$. To explore $SO_4^{\cdot-}$ generation mechanisms, the effect of $K_2S_2O_8$ concentrations of 5, 10, 15, 20, and 25 mmol·L^{-1} on the degradation of CIP in the US/$K_2S_2O_8$ system was investigated. The results of this analysis are shown in Figure 5.

Figure 5(a) shows that CIP removal efficiency varied over time under different $K_2S_2O_8$ concentrations. A breaking point occurred at 90 min in the 5 mmol·L^{-1} $K_2S_2O_8$ experimental group, at 60 and 30 min in the 10 mmol·L^{-1} $K_2S_2O_8$ and 15 mmol·L^{-1} $K_2S_2O_8$ experimental groups, respectively. Growth rates increased gradually with increasing reaction time after the breaking point. The increased removal efficiency in the 20 and 25 mmol·L^{-1} $K_2S_2O_8$ experimental groups were more

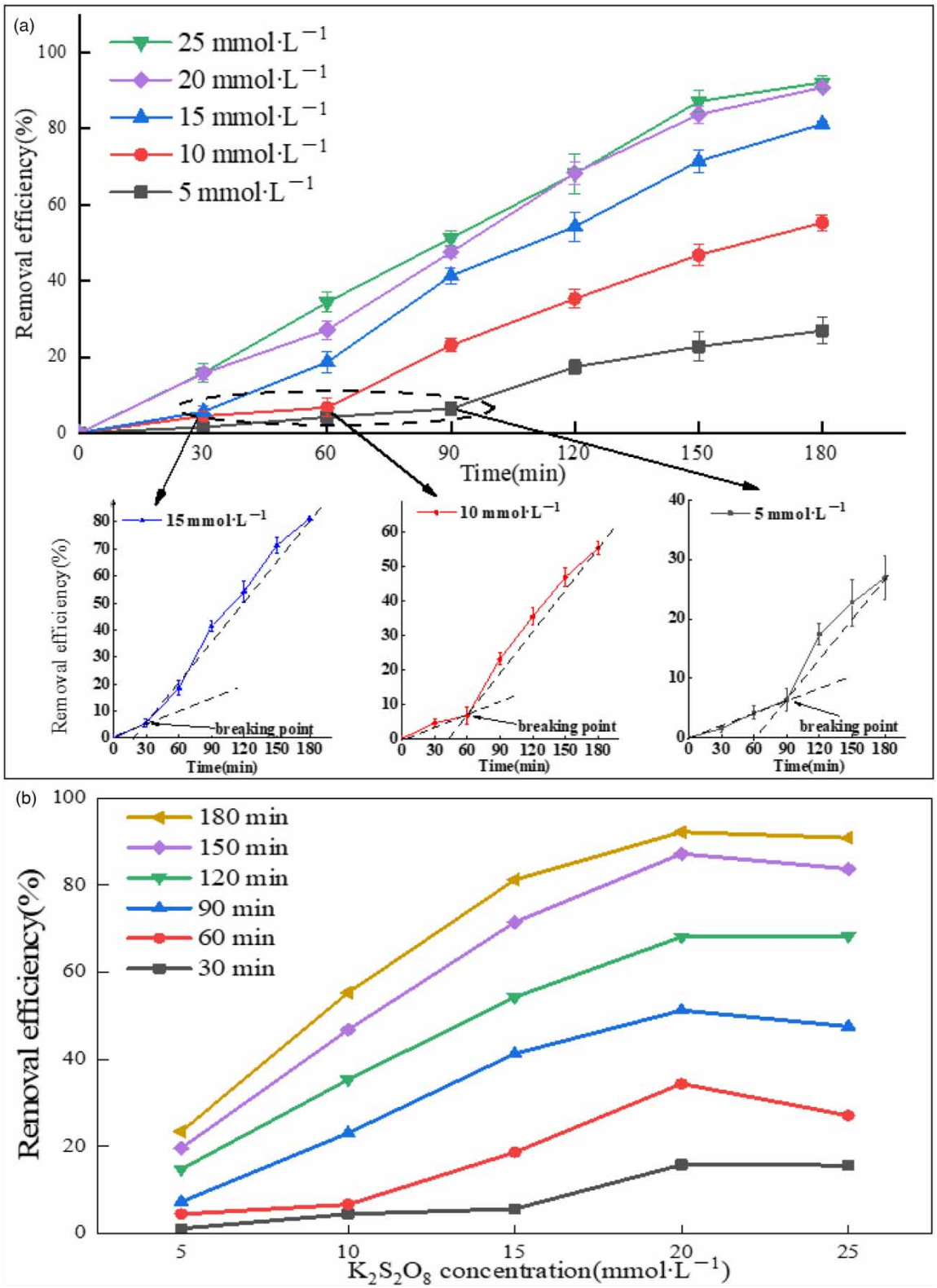

Figure 5 | (a) Relationship between the CIP removal efficiency and reaction time in the US/$K_2S_2O_8$ system with $K_2S_2O_8$ concentrations of 5, 10, 15, 20, and 25 mmol·L^{-1}; (b) relationship between CIP removal efficiency and the concentration of $K_2S_2O_8$ after different reaction times. Reaction conditions: CIP concentration = 20 mg·L^{-1}, frequency = 25 KHz, power = 360 W, pH = 7.

stable. CIP removal efficiency with different $K_2S_2O_8$ concentrations but the same reaction time are compared in Figure 5(b), showing that the removal efficiency was highest when $K_2S_2O_8$ concentrations were 20 mmol·L^{-1}. At $K_2S_2O_8$ concentrations lower than 20 mmol·L^{-1}, CIP removal efficiency increased with increasing $K_2S_2O_8$ concentration. However, a slight decrease in CIP degradation was observed when $K_2S_2O_8$ concentrations were increased up to 25 mmol·L^{-1}. At greater reaction times, the slope of the CIP removal curve gradually increased in the experimental group when $K_2S_2O_8$ concentrations were lower than 20 mmol·L^{-1} (Table S3), indicating that $K_2S_2O_8$ concentration positively influenced CIP removal efficiency.

In the 5, 10, and 15 mmol·L^{-1} $K_2S_2O_8$ experimental groups, few free radicals were generated during the initial stage of the reaction. Nonetheless, the high concentration of CIP led to the consumption of free radicals, which were insufficiently present to facilitate the chain reaction. As the reaction progressed, CIP concentrations decreased and free radicals gradually accumulated, thus a chain reaction was initiated, causing the generation of more free radicals in the system and their reaction with CIP. Consequently, a breaking point appeared in the removal efficiency growth rate that, at higher $K_2S_2O_8$ concentrations, appeared earlier. Under concentrations of 20 and 25 mmol·L^{-1} $K_2S_2O_8$, the chain reaction was initiated during the early stage of the reaction, and the removal rate increased rapidly. The above experimental phenomena cannot be explained only by the chain reaction, but also require that $K_2S_2O_8$ concentration had an important effect on the generation of $SO_4^{\cdot-}$.

During the initial stage of the reaction, $SO_4^{\cdot-}$ generation reached its maximum at a $K_2S_2O_8$ concentration of 20 mmol·L^{-1}, whereas $K_2S_2O_8$ concentrations exceeding 20 mmol·L^{-1} reduced CIP removal efficiency in the system due to the consumption of $SO_4^{\cdot-}$ by excess $K_2S_2O_8$ (Wang *et al.* 2014), as shown in Equation (10).

The above experimental results showed that ultrasonic power and the chain reaction provided two pathways for the generation of $SO_4^{\cdot-}$ in the US/$K_2S_2O_8$ system. $K_2S_2O_8$ concentration had an important effect on $SO_4^{\cdot-}$ generation, whereas high $K_2S_2O_8$ concentrations were not beneficial to the generation of $SO_4^{\cdot-}$.

Interaction between $SO_4^{\cdot-}$ and $HO^{\cdot}$ in the US/$K_2S_2O_8$ system

The above analyses show that ultrasonic power and the chain reaction are two main pathways by which $SO_4^{\cdot-}$ and $HO^{\cdot}$ are generated in the US/$K_2S_2O_8$ system. The role of US power has been well illustrated, but additional experimental evidence is required to support the chain reaction. From the definition of the chain reaction, it can be inferred that the relationship between $SO_4^{\cdot-}$ and $HO^{\cdot}$ entails that they increase or decrease synchronously. Experimental results relating to this problem can provide support to infer the chain reaction.

To address the above question and understand how to weaken the generation of $SO_4^{\cdot-}$ and $HO^{\cdot}$ in the US/$K_2S_2O_8$ system, changes in reaction effects were investigated and the mutual influence of $SO_4^{\cdot-}$ and $HO^{\cdot}$ was analyzed. Literature reports suggest that $SO_4^{\cdot-}$ is dominant under acidic conditions whereas $HO^{\cdot}$ predominated under basic conditions; however, both $SO_4^{\cdot-}$ and $HO^{\cdot}$ may predominate under neutral conditions (Liang *et al.* 2007). Therefore, the removal efficiency of CIP under various pH conditions (3, 5, 7, 9, and 11) was compared (Figure 6).

Figure 6 shows that differences in CIP removal efficiency were noted under different pH conditions, with the highest CIP removal efficiency at pH 7.

Under neutral conditions, $SO_4^{\cdot-}$ and $HO^{\cdot}$ coexist, allowing the chain reaction to proceed smoothly. This results in a wide variety of free radicals in the system and the highest CIP removal efficiency. At pH 3 and 5, although $SO_4^{\cdot-}$ was dominant, the conditions of $HO^{\cdot}$ generation were poor and the chain reaction did not proceed smoothly, resulting in decreased CIP removal efficiency. Similar phenomena were found at pH 9 and 11, i.e., although $HO^{\cdot}$ was dominant, the formation conditions of $SO_4^{\cdot-}$ were poor, resulting in decreased CIP removal efficiency. Under both acidic and basic conditions, the chain reaction was affected.

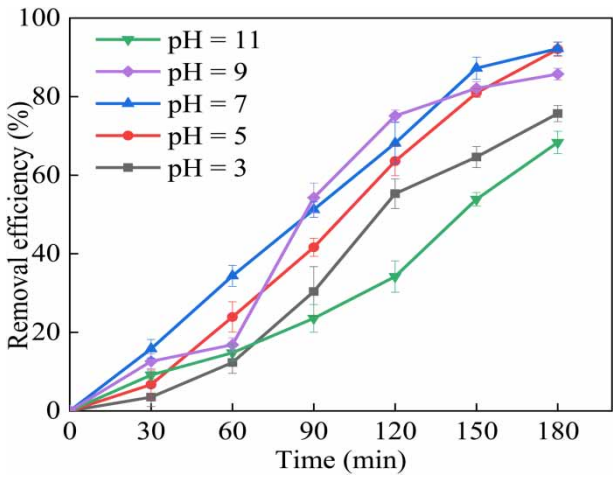

Figure 6 | Relationship between CIP removal efficiency and reaction time in the US/$K_2S_2O_8$ system at pH values of 3, 5, 7, 9, and 11. Reaction conditions: CIP concentration = 20 mg·L^{-1}, frequency = 25 KHz, $K_2S_2O_8$ concentration = 20 mmol·L^{-1}, power = 360 W.

Therefore, the above experimental results proved that, during the degradation of CIP in the US/$K_2S_2O_8$ system, both $SO_4^{\cdot-}$ and $HO^{\cdot}$ increased simultaneously *via* the chain reaction, while a decrease in the concentration of certain active free radicals affected the reaction efficiency of the entire system.

Free radical generation mechanism

According to the above analysis, CIP degradation in the US/$K_2S_2O_8$ system can be separated into the free radical generation stage and the reaction stage, as shown in Figure 7. The mechanism of free radical generation during the generation stage was as follows: (1) thermal dissociation of water caused by US cavitation leads to the generation of $HO^{\cdot}$; (2) generation of local high temperature and high pressure and activation of $K_2S_2O_8$ produces $SO_4^{\cdot-}$; (3) rising water temperature caused by US power leading the activation of $K_2S_2O_8$ and formation of $SO_4^{\cdot-}$; (4) when $HO^{\cdot}$ and $SO_4^{\cdot-}$ accumulated, the chain reaction was initiated, $HO^{\cdot}$ stimulated $K_2S_2O_8$ to form $SO_4^{\cdot-}$, and $SO_4^{\cdot-}$ continued to react with H_2O or OH^- to form $HO^{\cdot}$; (5) the excessive accumulation of $HO^{\cdot}$ resulted in $HO^{\cdot}$ quenching to form H_2O_2; (6) $SO_4^{\cdot-}$ quenching formed $S_2O_8^{2-}$ under conditions of excessive $SO_4^{\cdot-}$; and (7) too much $HO^{\cdot}$ and $SO_4^{\cdot-}$ reacted to form HSO_5^-.

Verification of the effects of $SO_4^{\cdot-}$ and $HO^{\cdot}$ over time

The degradation of CIP in the US/$K_2S_2O_8$ system involves complex reactions and the coexistence of multiple reactions. The main reaction type will vary depending upon reaction conditions. Both free radical generation and free radical reaction times are very short, thus only by correctly understanding free radical generation mechanisms can we predict the contribution of different free radicals in the degradation of CIP. Previous studies (Wei *et al.* 2017) have shown that the generation rate of $HO^{\cdot}$ in the US/$K_2S_2O_8$ system was faster than that of $SO_4^{\cdot-}$, but the survival time of $SO_4^{\cdot-}$ in aqueous solution (3×10^{-5}–4×10^{-5} s) was longer than that of $HO^{\cdot}$ (1×10^{-9} s) (Zhang *et al.* 2019). Figure 3(b) shows that $HO^{\cdot}$ generation conditions were most favorable during the early stage of the reaction and gradually weakened in the later stages. Figure 5(b) shows instead that the formation conditions of $SO_4^{\cdot-}$ were weak in the early stage of the reaction but gradually increased during the later stages. According to the above experimental phenomena and analysis of the free radical generation mechanisms outlined in the section on the free radical generation mechanism, we suggest that the action of $SO_4^{\cdot-}$ and $HO^{\cdot}$ changed with time. During the initial stages of the reaction, the degradation of CIP was dominated by $HO^{\cdot}$ oxidation. As the reaction proceeded, $HO^{\cdot}$ accumulated,

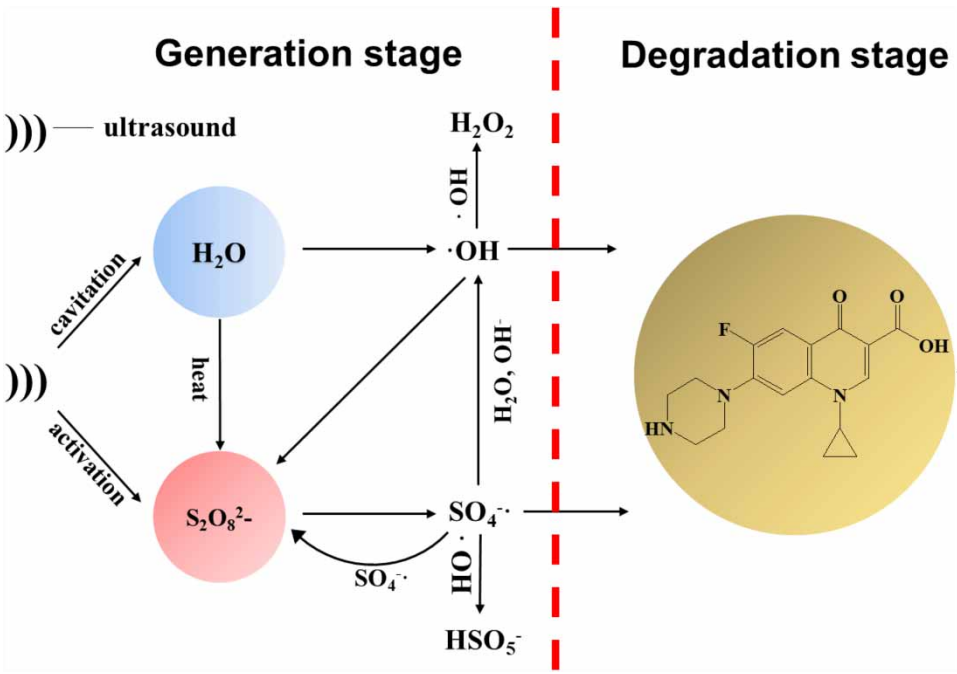

Figure 7 | Active free radical generation mechanism in the US/$K_2S_2O_8$ system.

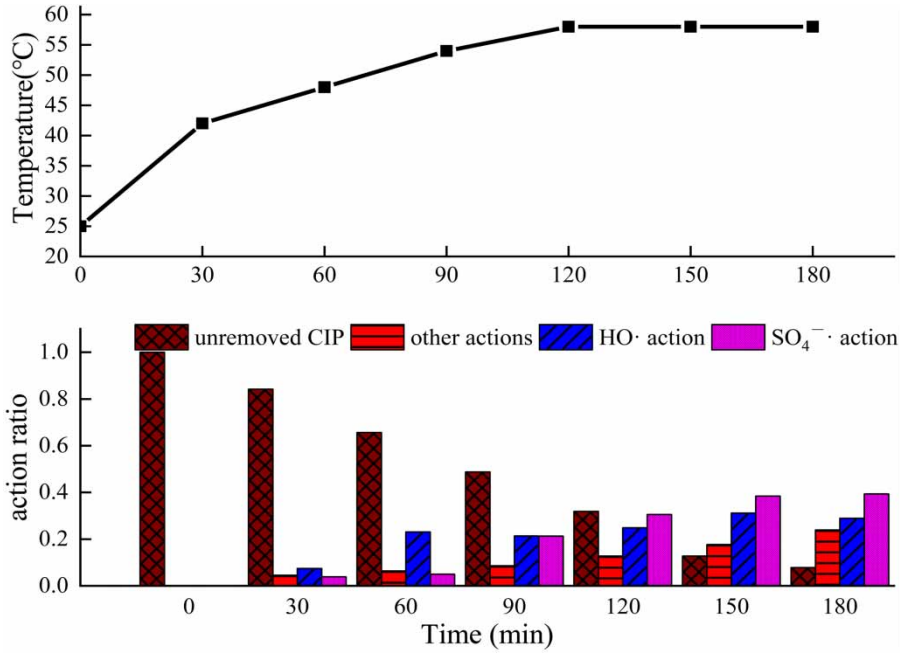

Figure 8 | Proportion of different actions in CIP degradation in the US/$K_2S_2O_8$ system.

the chain reaction was initiated, $S_2O_8^{2-}$ was excited and led to the formation of $SO_4^{-\bullet}$, and the proportion of $SO_4^{-\bullet}$ oxidation reactions in the system gradually increased.

To test the above theoretical conjecture, the experimental results shown in Figure 1 were calculated, and the effects of $SO_4^{-\bullet}$ and $HO^{\bullet}$ were quantified. The quality difference of CIP removal between the control group and the TBA experimental group reflected the removal quality due to $HO^{\bullet}$, whereas that between the TBA experimental group and the ISP experimental group reflected the removal quality due to $SO_4^{-\bullet}$. CIP removal quality in the isopropanol experimental group reflected the removal quality due to other actions. Previous research has demonstrated that the degradation mechanism of the US/PS system mainly involved the synergistic action of pyrolysis and free radicals, with relatively little effect from O^{2-} (Li *et al.* 2013). Here, the quenching experiment determined only the roles of $SO_4^{-\bullet}$ and $HO^{\bullet}$. In order to facilitate this study, the role of free radicals other than $SO_4^{-\bullet}$ and $HO^{\bullet}$, together with pyrolysis, were collectively referred to as other effects. The removal quality caused by the actions mentioned above and the residual quality were converted into a proportion of the initial addition quality, which indicated the proportion of $SO_4^{-\bullet}$ action, $HO^{\bullet}$ action, other action, and the unreacted part over different reaction times. This enabled the temperature of the system at different time points to be determined.

Figure 8 demonstrates that, after 180 min of reaction, the proportion of unremoved CIP was 7.80%, and the removed part (92.20%) was composed of $HO^{\bullet}$ action (28.90%), $SO_4^{-\bullet}$ action (39.37%) and other actions (23.93%). The action of $HO^{\bullet}$ on CIP degradation was rapid at first, but then slowed, whereas the $SO_4^{-\bullet}$ action on CIP degradation gradually increased over time. Before 90 min, the action of $HO^{\bullet}$ on CIP removal was higher than that of $SO_4^{-\bullet}$. The actions of $SO_4^{-\bullet}$ and $HO^{\bullet}$ were equal at 90 min (both 21%). After 90 min, $SO_4^{-\bullet}$ occupied a higher proportion of CIP removal than $HO^{\bullet}$. Our experimental results were consistent with the above conjecture.

Previous research (Zou *et al.* 2014) has shown that the $K_2S_2O_8$ peroxy bond was prone to breakage and to produce more $SO_4^{-\bullet}$ under high temperatures, whereas the dissolved oxygen in the system would decrease, resulting in a decrease in $HO^{\bullet}$ concentration (Yang *et al.* 2019). The above experimental results were in agreement with this change of temperature.

The experimental results shown in Figure 8 have verified the idea of changing roles of different free radicals in the reaction based the free radical generation mechanism described above, and have also demonstrated the proposed free radical generation mechanism.

CONCLUSIONS

Under the conditions of a CIP concentration of 20 $mg \cdot L^{-1}$, $K_2S_2O_8$ concentration of 20 $mmol \cdot L^{-1}$, US power of 360 W, and pH 7, CIP removal efficiency was 92.20% after

180 min, i.e., better than that of either the US system (14.63%) or the $K_2S_2O_8$ system (3.70%) when used alone. The synergistic effect in the US/$K_2S_2O_8$ system facilitated greater generation of $SO_4^{\cdot-}$ and $HO^{\cdot}$. The main mechanisms of free radical generation were US power and chain reaction. Cavitation effects caused by US power have been shown to promote the thermal dissociation of water to generate $HO^{\cdot}$ while activating $K_2S_2O_8$ to produce $SO_4^{\cdot-}$. With increasing water temperature, $K_2S_2O_8$ continued to be activated to form $SO_4^{\cdot-}$, leading to the accumulation of $HO^{\cdot}$ and $SO_4^{\cdot-}$ and eventually initiating a chain reaction in which $HO^{\cdot}$ stimulated $K_2S_2O_8$ to form $SO_4^{\cdot-}$; in turn, $SO_4^{\cdot-}$ continued to react with H_2O or OH^- to form $HO^{\cdot}$. During this process, $HO^{\cdot}$ and $SO_4^{\cdot-}$ increased or decreased simultaneously. The presence of $K_2S_2O_8$ can promote the generation of $HO^{\cdot}$, and the concentration of $K_2S_2O_8$ also had a significant positive effect for $SO_4^{\cdot-}$generation, although high concentrations were not beneficial. The quenching reaction occurs under high concentrations of $HO^{\cdot}$ and $SO_4^{\cdot-}$. During the initial stages of the reaction, the role of $HO^{\cdot}$ was more important than that of $SO_4^{\cdot-}$, whereas the role of $SO_4^{\cdot-}$ gradually increased as the reaction proceeded.

ACKNOWLEDGEMENTS

This work was supported by the National Natural Science Foundation of China (Grant no. 51908199), Key Scientific and Technological Project of Henan Province (Grant no. 172102310698).

DATA AVAILABILITY STATEMENT

All relevant data are included in the paper or its Supplementary Information.

REFERENCES

Ao, X. W., Liu, W. J., Sun, W. J., Cai, M. Q., Ye, Z., Yang, C., Lu, Z. D. & Li, C. 2018 Medium pressure UV-activated peroxymonosulfate for ciprofloxacin degradation: kinetics, mechanism, and genotoxicity. *Chem. Eng. J.* **345**, 87–97. https://doi.org/10.1016/j.cej.2018.03.133.

Avetta, P., Pensato, A., Minella, M., Malandrino, M., Maurino, V., Minero, C., Hanna, K. & Vione, D. 2015 Activation of persulfate by irradiated magnetite: implications for the degradation of phenol under heterogeneous photo-Fenton-like conditions. *Environ. Sci. Technol.* **49**, 1043–1050. https://doi.org/10.1021/es503741d.

Chen, W. S. & Huang, C. P. 2015 Mineralization of aniline in aqueous solution by electro-activated persulfate oxidation enhanced with ultrasound. *Chem. Eng. J.* **266**, 279–288. https://doi.org/10.1016/j.cej.2014.12.100.

Chen, W. S. & Huang, C. P. 2019 Mineralization of dinitrotoluenes in aqueous solution by sono-activated persulfate enhanced with electrolytes. *Ultrason. Sonochem.* **51**, 129–137. https://doi.org/10.1016/j.ultsonch.2018.10.035.

Darsinoua, B., Frontistisa, Z., Antonopouloub, M., Konstantinoub, L. & Mantzavinosa, D. 2015 Sono-activated persulfate oxidation of bisphenol A: kinetics, pathways and the controversial role of temperature. *Chem. Eng. J.* **280**, 623–633. https://doi.org/10.1016/j.cej.2015.06.061.

Ferkous, H., Merouani, S., Hamdaoui, O. & Petrier, C. 2017 Persulfate-enhanced sonochemical degradation of naphthol blue black in water: evidence of sulfate radical formation. *Ultrason. Sonochem.* **34**, 580–587. https://doi.org/10.1016/j.ultsonch.2016.06.027.

Gao, Y. Q., Gao, N. Y., Wang, W., Kang, S. F., Xu, H. J. & Yin, D. Q. 2018 Ultrasound-assisted heterogeneous activation of persulfate by nano zero-valent iron (nZVI) for the propranolol degradation in water. *Ultrason. Sonochem.* **49**, 33–40. https://doi.org/10.1016/j.ultsonch.2018.07.001.

Gao, J., Han, D. Q., Xu, Y., Liu, Y. Y. & Shang, J. G. 2020 Persulfate activation by sulfide-modified nanoscale iron supported by biochar (S-nZVI/BC) for degradation of ciprofloxacin. *Sep. Sci. Technol.* **235**, 116202. https://doi.org/10.1016/j.seppur.2019.116202.

Hao, F. F., Guo, W. L., Wang, A. Q., Leng, Y. Q. & Li, H. L. 2014 Intensification of sonochemical degradation of ammonium perfluorooctanoate by persulfate oxidant. *Ultrason. Sonochem.* **21**, 554–558. https://doi.org/10.1016/j.ultsonch.2013.09.016.

House, D. A. 1962 Kinetics and mechanism of oxidations by peroxydisulfate. *Chem. Rev.* **62**, 185–203. https://doi.org/10.1021/cr60217a001.

Huang, K. C., Couttenye, R. A. & Hoag, G. E. 2002 Kinetics of heat-assisted persulfate oxidation of methyl tert-butyl ether (MTBE). *Chemosphere* **49**, 413–420. https://doi.org/10.1016/S0045-6535(02)00330-2.

Laat, D. T. & Gallard, H. 1999 Catalytic decomposition of hydrogen peroxide by Fe (III) in homogeneous aqueous solution: mechanism and kinetic modeling. *Environ. Sci. Technol.* **33**, 2726–2732. https://doi.org/10.1021/es981171v.

Lei, Y. J., Tian, Y., Fang, C., Zhan, W., Duan, L. C., Zhang, J., Zuo, W. & Kong, X. W. 2019 Insights into the oxidation kinetics and mechanism of diesel hydrocarbons by ultrasound activated persulfate in a soil system. *Chem. Eng. J.* **378**, 122253. https://doi.org/10.1016/j.cej.2019.122253.

Li, M., Wei, D. B., Zhao, H. M. & Du, Y. G. 2013 Genotoxicity of quinolones: substituents contribution and transformation products QSAR evaluation using 2D and 3D models. *Chemosphere* **95**, 220–226. https://doi.org/10.1016/j.chemosphere.2013.09.002.

Li, Z. L., Guo, C. S., Lyu, J. Y., Hu, Z. & Ge, M. 2019 Tetracycline degradation by persulfate activated with magnetic Cu/

$CuFe_2O_4$ composite: efficiency, stability, mechanism and degradation pathway. *J. Hazard. Mater.* **373**, 85–96. https://doi.org/10.1016/j.jhazmat.2019.03.075.

Liang, C. J., Wang, Z. S. & J. Bruellb, C. 2007 Influence of pH on peroxydisulfate oxidation of TCE at ambient temperatures. *Chemosphere* **66**, 106–113. https://doi.org/10.1016/j.chemosphere.2006.05.026.

Liu, Y. Q., He, X. X. & Fu, Y. S. 2016 Kinetics and mechanism investigation on the destruction of oxytetracycline by UV-254 nm activation of persulfate. *J. Hazard. Mater.* **305**, 229–239. https://doi.org/10.1016/j.jhazmat.2015.11.043.

Matzek, L. W. & Carter, K. E. 2016 Activated persulfate for organic chemical degradation: a review. *Chemosphere* **151**, 178–188. https://doi.org/10.1016/j.chemosphere.2016.02.055.

Milh, H., Schoenaers, B., Stesmans, A., Cabooter, D. & Dewil, R. 2020 Degradation of sulfamethoxazole by heat-activated persulfate oxidation: elucidation of the degradation mechanism and influence of process parameters. *Chem. Eng. J.* **379**, 122234. https://doi.org/10.1016/j.cej.2019.122234.

Monteagudo, J. M., Durán, A., González, R. & Expósito, A. J. 2015 In situ chemical oxidation of carbamazepine solutions using persulfate simultaneously activated by heat energy, UV light, Fe^{2+} ions, and H_2O_2. *Appl. Catal. B.* **176–177**, 120–129. https://doi.org/10.1016/j.apcatb.2015.03.055.

Monteagudo, J. M., Taliawy, H. E., Durána, A., Caroa, G. & Besterb, K. 2018 Sono-activated persulfate oxidation of diclofenac: degradation, kinetics, pathway and contribution of the different radicals involved. *J. Hazard. Mater.* **357**, 457–465. https://doi.org/10.1016/j.jhazmat.2018.06.031.

Nasseri, S., Mahvi, A. H., Seyedsalehi, M., Yaghmaeianac, M., Nabizadehae, R., Alimohammadia, M. & Safari, G. H. 2017 Degradation kinetics of tetracycline in aqueous solutions using peroxydisulfate activated by ultrasound irradiation: effect of radical scavenger and water matrix. *J. Mol. Liq.* **241**, 704–714. https://doi.org/10.1016/j.molliq.2017.05.137.

Qian, Y., Xue, G. & Chen, J. 2018 Oxidation of cefalexin by thermally activated persulfate kinetics, products, and antibacterial activity change. *J. Hazard. Mater.* **354**, 153–160. https://doi.org/10.1016/j.jhazmat.2018.05.004.

Sharma, J., Mishra, I. M. & Kumar, V. 2016 Mechanistic study of photo-oxidation of Bisphenol-A (BPA) with hydrogen peroxide (H_2O_2) and sodium persulfate (SPS). *J. Environ. Manage.* **166**, 12–22. https://doi.org/10.1016/j.jenvman.2015.09.043.

Song, W. H., Armah A, D. L. C., Rein, K. & O'Shea, K. E. 2006 Ultrasonically induced degradation of microcystin-LR and -RR: identification of products, effect of pH, formation and destruction of peroxides. *Environ. Sci. Technol.* **40**, 3941–3946. https://doi.org/10.1021/es0521730.

Suslick, K. S. 1990 Sonochemistry. *Science* **247**, 1439–1445. https://doi.org/10.1126/science.247.4949.1439.

Tang, L., Liu, Y. N., Wang, J. J., Zeng, G. M., Deng, Y. C., Deng, H. Y., Dong, H. R., Feng, H. P., Wang, J. J. & Peng, B. 2018 Enhanced activation process of persulfate by mesoporous carbon for degradation of aqueous organic pollutants: electron transfer mechanism. *Appl. Catal. B.* **231**, 1–10. https://doi.org/10.1016/j.apcatb.2018.02.059.

Wang, X., Wang, L., Li, J. B., Qiu, J. J., Cai, C. & Zhang, H. 2014 Degradation of Acid Orange 7 by persulfate activated with zero valent iron in the presence of ultrasonic irradiation. *Sep. Sci. Technol.* **122**, 41–46. https://doi.org/10.1016/j.seppur.2013.10.037.

Wang, S. L., Zhou, N., Wu, S. & Zhang, Q. 2015 Modeling the oxidation kinetics of sono-activated persulfate's process on the degradation of humic acid. *Ultrason. Sonochem.* **23**, 128–134. https://doi.org/10.1016/j.ultsonch.2014.10.026.

Wang, Q., Cao, Y., Zeng, H., Liang, Y. H., Ma, J. & Lu, X. H. 2019a Ultrasound-enhanced zero-valent copper activation of persulfate for the degradation of bisphenol AF. *Chem. Eng. J.* **335**, 122143. https://doi.org/10.1016/j.cej.2019.122143.

Wang, S. L., Wu, J. F., Lu, X. Q., Xu, W. X., Gong, Q., Ding, J. Q., Dan, B. S. & Xie, P. C. 2019b Removal of acetaminophen in the Fe^{2+}/persulfate system: kinetic model and degradation pathways. *Chem. Eng. J.* **358**, 1091–1100.

Wei, Z., Villamena, F. A. & Weavers, L. K. 2017 Kinetics and mechanism of ultrasonic activation of persulfate: an in situ EPR spin trapping study. *Environ. Sci. Technol.* **51**, 3410–3417. https://doi.org/10.1021/acs.est.6b05392.

Yang, L., Xue, J. M., He, L. Y., Wu, L., Ma, Y. F., Chen, H., Li, H., Peng, P. & Zhang, Z. L. 2019 Review on ultrasound assisted persulfate degradation of organic contaminants in wastewater: influences, mechanisms and prospective [J]. *Chem. Eng. J.* **378**, 122146. https://doi.org/10.1016/j.cej.2019.122146.

Yen, C. H., Chen, K. F., Kao, C. M., Liang, S. H. & Chen, T. Y. 2011 Application of persulfate to remediate petroleum hydrocarbon-contaminated soil: feasibility and comparison with common oxidants. *J. Hazard. Mater.* **186**, 2097–2102. https://doi.org/10.1016/j.jhazmat.2010.12.129.

Yousefi, N., Pourfadakaribc, S., Esmaeili, S. & Babaei, A. A. 2019 Mineralization of high saline petrochemical wastewater using sonoelectro-activated persulfate: degradation mechanisms and reaction kinetics. *Microchem. J.* **147**, 1075–1082. https://doi.org/10.1016/j.microc.2019.04.020.

Zhang, Z. M. & Zheng, H. L. 2009 Optimization for decolorization of azo dye acid green 20 by ultrasound and H_2O_2 using response surface methodology. *J. Hazard. Mater.* **177**, 1388–1393. https://doi.org/10.1016/j.jhazmat.2009.07.146.

Zhang, P., Tan, X. F., Liu, S. B., Liu, Y. G., Zeng, G. M., Ye, S. J., Yin, Z. H., Hu, X. J. & Liu, N. 2019 Catalytic degradation of estrogen by persulfate activated with iron-doped graphitic biochar: process variables effects and matrix effects. *Chem. Eng. J.* **378**, 122141. https://doi.org/10.1016/j.cej.2019.122141.

Zou, X. L., Zhou, T., Mao, J. & Wu, X. H. 2014 Synergistic degradation of antibiotic sulfadiazine in a heterogeneous ultrasound-enhanced Fe^0/persulfate Fenton-like system. *Chem. Eng. J.* **257**, 36–44. https://doi.org/10.1016/j.cej.2014.07.048.

First received 22 January 2021; accepted in revised form 25 March 2021. Available online 1 April 2021